

Pulsed Laser Deposition of High-Quality Thin Films of the Insulating Ferromagnet EuS

Qi I. Yang,^{1,2,3, a)} Jinfeng Zhao,⁴ Li Zhang,^{3,5} Merav Dolev,^{3,5} Alexander D. Fried,^{1,3} Ann F. Marshall,⁶ Subhash H. Risbud,⁴ and Aharon Kapitulnik^{1,2,3,5}

¹⁾ *Department of Physics, Stanford University, Stanford, CA 94305*

²⁾ *Stanford Institute for Materials and Energy Sciences, SLAC National Accelerator Laboratory, 2575 Sand Hill Road, Menlo Park, California 94025, USA*

³⁾ *Geballe Laboratory for Advanced Materials, Stanford University, Stanford, CA 94305*

⁴⁾ *Department of Chemical Engineering and Materials Science, University of California, Davis, CA 95616*

⁵⁾ *Department of Applied Physics, Stanford University, Stanford, CA 94305*

⁶⁾ *Stanford Nanocharacterization Laboratory, Stanford University, Stanford, CA 94305*

(Dated: 7 June 2021)

High-quality thin films of the ferromagnetic insulator europium(II) sulfide (EuS) were fabricated by pulsed laser deposition on Al₂O₃ (0001) and Si (100) substrates. A single orientation was obtained with the [100] planes parallel to the substrates, with atomic-scale smoothness indicates a near-ideal surface topography. The films exhibit uniform ferromagnetism below 15.9 K, with a substantial component of the magnetization perpendicular to the plane of the films. Optimization of the growth condition also yielded truly insulating films with immeasurably large resistance. This combination of magnetic and electric properties open the gate for novel devices that require a true ferromagnetic insulator.

Over more than 50 years a wealth of new effects and properties have been discovered in binary lanthanide compounds. In particular, compounds of europium with elements of the sixth group (O,S,Se,Te) exhibit a rock-salt (NaCl)-type crystal structure with ordered magnetic states at low temperatures. As the lattice parameter increases from EuO to EuTe, a ferromagnetic ordered state of moments localized on Eu ions appear in EuO ($T_C \approx 69$ K) and in EuS ($T_C \approx 16.7$ K),^{1,2} while EuSe and EuTe show collinear antiferromagnetic ordering with $T_N \approx 4.2$ K, $T_N \approx 9.8$ K respectively.^{3,4} In these chalcogenide compounds, the S ground state of Eu²⁺ ions and their simple face centered cubic (FCC) magnetic lattice facilitate testings of the Heisenberg model of ferromagnetism and theories of critical phenomena.⁵⁻⁹ A variety of applications were proposed or implemented utilizing these magnetic semiconductors.¹⁰⁻¹² A class of magnetoelectric applications, such as π -Josephson junctions for quantum qubits¹³⁻¹⁵ and recently proposed topological magnetoelectric effect associated with the surface state of topological insulators,¹⁶⁻²⁰ require fabrication of high-quality insulating ferromagnet thin films with robust magnetic properties.

Here we focus on EuS, which is a semiconductor with an indirect energy gap between the 4f⁷ Eu states and the conduction band minimum at 300 K is 1.65 eV.²¹⁻²³ The lattice parameter of bulk crystals of EuS is $a_0 = 5.967$ Å, with a ferromagnetic Curie temperature $T_C \approx 16.7$ K. When strained, the lattice constant change is accompanied by a change in Curie temperature, e.g. thin films of EuS grown on KCl show an increase in T_C by as much as 2 K, due to compression induced by differential expan-

sions of the film and substrate.²⁴ At the same time, very thin films will exhibit slightly lower T_C due to dimensionality reduction.²⁵ However, although good electric insulation ($\rho \sim 10^4$ Ω·cm) was obtained in high-quality single crystals, difficulties in material fabrication lead to disorder and unintentional doping, which may drastically reduce the resistivity to as low as $\rho \sim 10^{-2}$ Ω·cm.^{2,26} Such reduction in resistivity was found to be accompanied by increased Curie temperatures due to interactions between charge carriers and the Eu²⁺ ions.^{1,26-28} Particularly for thin films, samples fabricated by either pulsed laser deposition (PLD) or molecular beam epitaxy (MBE) were reported to have T_C higher than single crystal values and were suggested to have significant carrier doping.²⁹⁻³¹ In addition, all reported growth methods³⁰⁻³² resulted in samples with multiple crystal orientations,³⁰⁻³² which might give rise to fractured magnetic domains given the considerable magnetocrystalline anisotropy of EuS.³³

In this Letter we present results of PLD-grown EuS thin films with significantly improved qualities related to surface topography, magnetic anisotropy, and electrical insulation, all of critical importance for applications involving interfacing the EuS film with another system. Specifically we show characterization results indicating excellent electric insulation, significant and uniform out-of-plane component of the magnetization, a single crystal orientation and a near-ideal surface topography. These improvements should facilitate a series of applications, such as topological insulator-ferromagnet bilayer devices.²⁰

For PLD targets, solid disks (approximately 19 mm in diameter and 3 mm thick) were prepared from high-purity (99.95%) EuS powder by a fast consolidation technique popularly referred to as spark plasma sintering (SPS). This technique uses an electric discharge to ac-

^{a)} Electronic mail: qiyang@stanford.edu

tivate the surface of the powder particles prior to rapid resistance heating aimed at achieving complete densification. SPS has been effectively used to make solid disk-like targets of a wide range of materials including chalcogenides^{34,35} and its efficiency in forming clean grain boundaries in polycrystalline targets has been shown for nitrides and refractory high-temperature materials.^{36,37} The target surface was polished with a 800 grit diamond sandpaper before transferring to high vacuum. For final conditioning of the target surface and to deposit EuS thin films, the target was ablated by a 25 ns 248 nm KrF excimer pulsed laser beam in $p = 6 \times 10^{-7}$ Torr high vacuum at 10 Hz repetition rate. The typical ablation spot size was $2.1 \pm 0.3 \text{ mm}^2$ and the measured fluences were $1.0 \pm 0.2 \text{ J} \cdot \text{cm}^{-2}$. Corundum Al_2O_3 (0001) and Si (100) substrates were cleaned *ex situ* by solvent sonication prior to transfer to high vacuum. The substrates were heated to 650 °C and placed 5 cm away from the target at the center of the plasma plume. The growth rate was estimated to be 1.3 Å per pulse. After each deposition, the substrates were cooled in vacuum to 60 °C with a rate slower than 15 °C/min.

The resultant thin films with thicknesses $20 \text{ nm} < t < 200 \text{ nm}$ have a translucent purple color on Al_2O_3 and are dark green on Si. Fig. 1a shows a transmission electron micrograph (TEM) of a thin film cross-section where the FCC lattice of EuS can be clearly observed. The lattice constant is estimated from direct length mea-

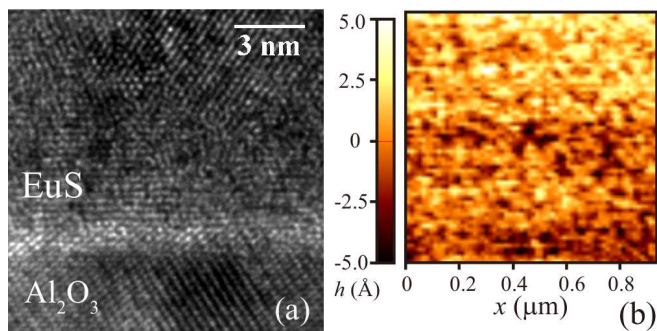


FIG. 1. (a) Cross-sectional TEM image of an EuS thin film, showing its interface to the Al_2O_3 (0001) substrate. (b) AFM image of a $1 \mu\text{m} \times 1 \mu\text{m}$ area showing the surface topography of a 20 nm EuS film. The root-mean-square roughness of $\sigma = 1.8 \text{ \AA}$ indicates smoothness to the atomic scale.

surements to be $a = 6.0 \pm 0.2 \text{ \AA}$, consistent with the established results.² Surface topography was measured with an atomic force microscope (AFM). Fig. 1b shows a $1 \mu\text{m} \times 1 \mu\text{m}$ area on the surface of a 20 nm film on Al_2O_3 . The difference between the minima and maxima in height is roughly twice the lattice constant. The root-mean-square roughness $\sigma = 1.8 \text{ \AA}$ calculated from a randomly selected line profile indicates near-ideal smoothness. Similar smoothness were obtained on films with thicknesses up to 200 nm deposited on either Al_2O_3 (0001) or Si (100).

Fig. 2 shows the X-ray diffraction patterns on the PLD

grown EuS thin films. On both Al_2O_3 (0001) and Si (100)

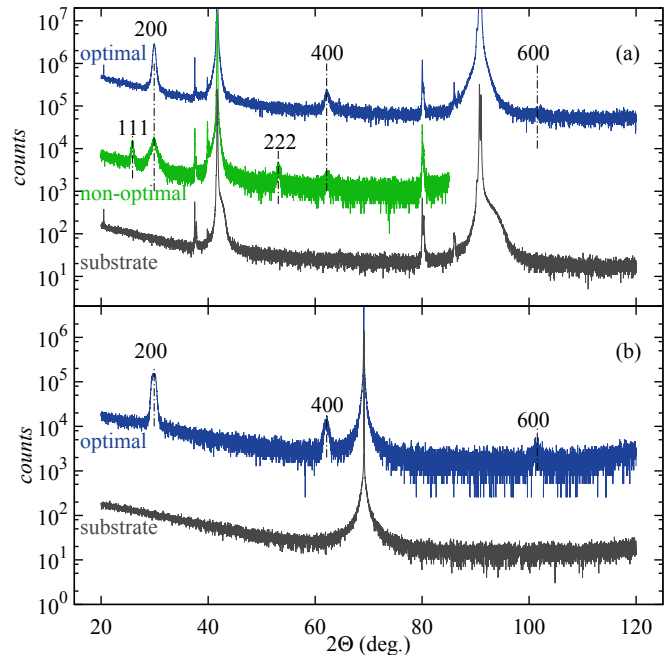


FIG. 2. Semi-log X-ray diffraction patterns of 20 nm EuS thin films. (a) On Al_2O_3 (0001) substrates, optimal growth conditions lead to a single (100) orientation, whereas multiple orientations were observed on non-optimal conditions. Spikes near substrate peaks are due to the K- β components of the X-ray source. (b) On Si (100) substrates with native oxides, single (100) orientation was obtained at optimal growth conditions. To distinguish the EuS (400) peak, a monochromator was used in the Si (100) case to eliminate the K- β components. (Please see the text for growth conditions.)

substrates, the optimal conditions described earlier produced samples with a single orientation where the [100] planes are parallel to the substrate surface. On Al_2O_3 (0001) substrates (fig. 2a), the (200) and (400) reflections are easily identified whereas the (600) reflection is discernible from the background. On Si (100) substrates (fig. 2b), all [100] reflections are clearly observable. For comparison, the diffraction pattern of a non-optimal sample deposited on Al_2O_3 (0001) at a lower temperature ($T = 600 \text{ }^\circ\text{C}$) was plotted in fig. 2a. Reflections from both the [100] and the [111] orientations were observed with comparable weights. Similar multiple orientations were observed in samples deposited at higher-than-optimal temperatures ($T > 700 \text{ }^\circ\text{C}$) or higher ambient pressures ($p > 2 \times 10^{-6}$ Torr).

The resistances of the EuS thin films were measured with a Van der Pauw technique.³⁸ When deposited at the optimal conditions on either Al_2O_3 (0001) or Si (100) substrates, samples with thicknesses $20 \text{ nm} < t < 200 \text{ nm}$ all show sheet resistances $R_{\square} > 20 \text{ M}\Omega$ at temperatures $T > 100 \text{ K}$, and immeasurably high resistance at lower temperatures. This is equivalent to bulk resistivity exceeding $\rho > 400 \text{ } \Omega \cdot \text{cm}$, consistent to values obtained on high-purity single crystals.² In contrast, films deposited

at non-optimal conditions show sheet resistances as low as $R_{\square} \sim \text{k}\Omega$ (fig. 3a), which corresponds to a bulk re-

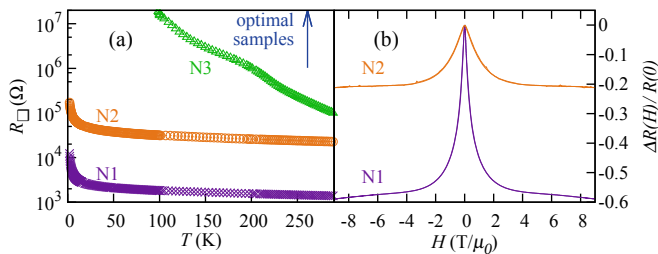


FIG. 3. (a) While samples grown at optimal conditions have sheet resistance $R_{\square} > 20 \text{ M}\Omega$ for $2 \text{ K} < T < 300 \text{ K}$, samples grown under non-optimal conditions (N1–N3, with 200 nm thickness) show finite resistance, indicating high carrier densities. (b) These non-optimal samples show negative giant magnetoresistance at $T = 2 \text{ K}$, similar to that observed in n-type single crystals.

sistivity of $\rho \sim 10^{-2} \Omega \cdot \text{cm}$, consistent with the conductive régime in doped single crystals.²⁶ Different from n-type single crystals results, where resistance anomalies were observed near T_C and attributed to change in carrier concentrations,^{26,28} monotonic increases in resistance were observed towards low temperatures in thin films. Such difference could be resulted from different natures of dopants or due to the effects of reduced dimensionality.³⁹ Similar to n-type doped single crystals, negative giant magnetoresistance was observed in conducting samples at low temperatures (fig. 3b).

Magnetizations of the thin films were measured in a superconducting quantum interference device (SQUID) magnetometer down to $T = 2 \text{ K}$. A significant perpendicular component of the magnetization was observed (fig. 4a), whereas the easy axes are in the sample plane (fig. 4b). While the coercive field of perpendicular magnetization may vary within the same order of magnitude for film thicknesses between 20 nm and 200 nm, the general hysteresis features are similar for all our samples on either Al_2O_3 (0001) or Si (100). By fitting to the Curie-Weiss law in the paramagnetic regime (fig. 4c), an upper limit of the Curie temperature of an optimal 20 nm thin film on Al_2O_3 (0001) was estimated to be $T_C = 15.9 \text{ K}$.⁴⁰ While a low T_C is expected for samples with diminishing carrier densities,^{1,26,28} we note that the thin film T_C is lower than the minimal single crystal value $T_C \approx 16.5 \text{ K}$. This is likely a combined effect of polycrystallinity, approaching the two-dimensional limit and lattice strains.^{41–43}

To test for homogeneity of the magnetism in our films we used a scanning Sagnac interferometer.⁴⁴ This device is based on a zero-area loop Sagnac interferometer as was first demonstrated by Xia *et al.*,⁴⁵ and can measure the Polar Kerr angle upon reflection from the film with shot-noise limited sensitivity at low power. Our scanning device is operated at a wavelength of 820 nm, and has a spatial resolution of $0.9 \mu\text{m}$. Fig. 4d shows several line scans of length $100 \mu\text{m}$, taken at a temperature of

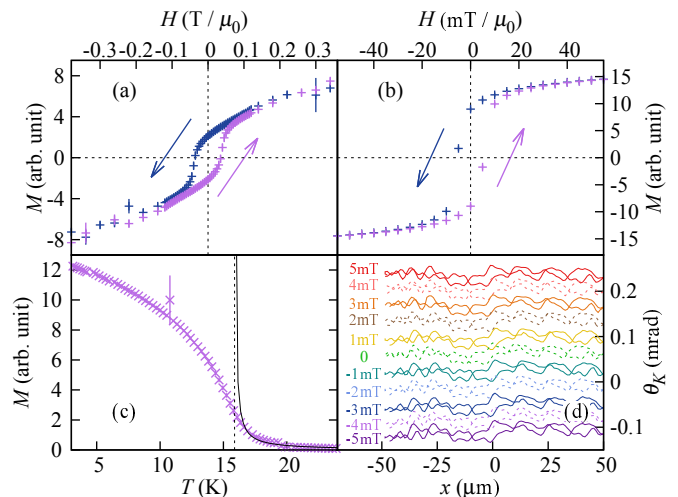


FIG. 4. Magnetization of a 20 nm EuS film on Al_2O_3 (0001), (a) in perpendicular fields, (b) in parallel fields, and (c) its temperature dependence, plotted in the same arbitrary unit with a linear paramagnetic component of the substrate subtracted. The fitting to the Curie-Weiss Law indicates a low Curie temperature $T_C = 15.9 \text{ K}$. (d) Kerr effect measured with a scanning Sagnac interferometer at $T = 10 \text{ K}$, showing uniform magnetization.

10 K and at low magnetic fields, showing a very uniform Kerr response. This set of line scans also agrees with the coercive field found in the SQUID magnetometry measurements.

While the experimental setup for PLD is relatively simple, it is well known that complex and non-equilibrium mechanisms are involved in both laser ablation of the target and plume-substrate interactions. Here we present a tentative discussion on the growth process. At the optimal growth conditions, the resultant atomically smooth topography seems to suggest the Frank–van der Merwe mode of nucleation. The absence of microstructures, which indicates sufficient reduction of partial evaporation (“splashing”),⁴⁶ may have been in part due to the effective densification with the SPS technique and appropriate target surface treatment. While EuS solid is stable up to $2300 \text{ }^\circ\text{C}$ in vacuum,⁴⁷ we found that the film quality is sensitive to relatively small deviations ($\Delta T = \pm 50 \text{ }^\circ\text{C}$) from the optimal substrate temperature $T = 650 \text{ }^\circ\text{C}$. Lowering the substrate temperature or increasing the ambient pressure are known to increase the cooling rate of adatoms. For compounds with large differences in constituent elements’ vapor pressures such as EuS, ($p(\text{S})/p(\text{Eu}) > 10^4$ at $T = 650 \text{ }^\circ\text{C}$,⁴⁸) such effects worsen both stoichiometry and structure.⁴⁹ In addition, the detrimental effects of changing temperature at either directions may be related to the nearby eutectic point at $750 \text{ }^\circ\text{C}$ and the EuS_2 phase below $575 \text{ }^\circ\text{C}$,⁴⁷ which may provide transient states that facilitate structural distortions or an Eu-rich stoichiometry. In either case, the distortion in stoichiometry would likely result in unintended doping.

To summarize, high-quality thin films of EuS were fabricated by pulsed laser deposition. Single (100) orientation and atomic-scale surface smoothness ($\sigma = 1.8 \text{ \AA}$) were obtained. Samples deposited at optimal conditions are highly insulating with sheet resistance $R_{\square} > 20 \text{ M}\Omega$ for thickness $20 \text{ nm} < t < 200 \text{ nm}$. Significant magnetizations were observed at the out-of-plane direction, showing hysteresis and homogeneous spatial distribution. These properties are crucial for various magnetoelectric applications. For comparison, we demonstrated that samples deposited at non-optimal conditions show low resistance and negative giant magnetoresistance, indicating unintended doping, possibly due to distorted composition stoichiometry.

ACKNOWLEDGMENTS

We would like to thank Robert Hammond, Min Liu, Di Lu, Alexander Palevski, Elizabeth Schemm, Arturas Vailionis and Philip Wu for help and discussions. This work is supported by DARPA, MesoDynamic Architecture Program (MESO) through the contract number N66001-11-1-4105, by FENA, and by a seed grant from DOE for the study of TI. A series of open-source software have been utilized during data analysis.^{50,51}

- ¹M. W. Shafer and T. R. McGuire, *Journal of Applied Physics* **39**, 588 (1968).
- ²M. Shafer, *Materials Research Bulletin* **7**, 603 (1972).
- ³P. Fischer, W. Hlg, W. Wartburg, P. Schwob, and O. Vogt, *Physik der kondensierten Materie* **9**, 249 (1969).
- ⁴G. Busch, P. Junod, R. Morris, J. Muheim, and W. Stutius, *Physics Letters* **11**, 9 (1964).
- ⁵T. R. McGuire, B. E. Argyle, M. W. Shafer, and J. S. Smart, *Journal of Applied Physics* **34**, 1345 (1963).
- ⁶P. J. Wojtowicz, *Journal of Applied Physics* **35**, 991 (1964).
- ⁷P. Boni, G. Shirane, H. G. Bohn, and W. Zinn, *Journal of Applied Physics* **61**, 3397 (1987).
- ⁸H. G. Bohn, A. Kollmar, and W. Zinn, *Phys. Rev. B* **30**, 6504 (1984).
- ⁹S. H. Charap and E. L. Boyd, *Phys. Rev.* **133**, A811 (1964).
- ¹⁰L. Esaki, P. J. Stiles, and S. v. Molnar, *Phys. Rev. Lett.* **19**, 852 (1967).
- ¹¹M. R. Freeman, "Fiber optic probe with a magneto-optic film on an end surface for detecting a current in an integrated circuit," (1995), US Patent 5,451,863.
- ¹²M. Müller, M. Luysberg, and C. M. Schneider, *Applied Physics Letters* **98**, 142503 (2011).
- ¹³T. Yamashita, K. Tanikawa, S. Takahashi, and S. Maekawa, *Phys. Rev. Lett.* **95**, 097001 (2005).
- ¹⁴L. Bulaevskii, V. Kuzii, and A. Sobyenin, *JETP Lett.* **25**, 290 (1977).
- ¹⁵J. Xia, V. Shelukhin, M. Karpovski, A. Kapitulnik, and A. Palevski, *Phys. Rev. Lett.* **102**, 087004 (2009).
- ¹⁶R. Yu, W. Zhang, H.-J. Zhang, S.-C. Zhang, X. Dai, and Z. Fang, *Science* **329**, 61 (2010).
- ¹⁷I. Garate and M. Franz, *Phys. Rev. Lett.* **104**, 146802 (2010).
- ¹⁸W. Luo and X.-L. Qi, *Phys. Rev. B* **87**, 085431 (2013).
- ¹⁹M. Snelder, M. Veldhorst, A. A. Golubov, and A. Brinkman, *Phys. Rev. B* **87**, 104507 (2013).
- ²⁰Q. I. Yang, M. Dolev, L. Zhang, J. Zhao, A. D. Fried, E. Schemm, M. Liu, A. Palevski, A. F. Marshall, S. H. Risbud, and A. Kapitulnik, *Phys. Rev. B* **88**, 081407 (2013).
- ²¹G. Busch, P. Junod, and P. Wachter, *Physics Letters* **12**, 11 (1964).
- ²²S. J. Cho, *Phys. Rev.* **157**, 632 (1967).
- ²³W. Müller and W. Nolting, *Phys. Rev. B* **66**, 085205 (2002).
- ²⁴A. Stachow-Wójcik, T. Story, W. Dobrowolski, M. Arciszewska, R. R. Galazka, M. W. Kreijveld, C. H. W. Swüste, H. J. M. Swagten, W. J. M. de Jonge, A. Twardowski, and A. Y. Sipatov, *Phys. Rev. B* **60**, 15220 (1999).
- ²⁵J. Keller, J. Parker, J. Stankiewicz, D. Read, P. Stampe, R. Kennedy, P. Xiong, and S. von Molnar, *IEEE Transactions on Magnetics* **38**, 2673 (2002).
- ²⁶Y. Shapira and T. B. Reed, *Phys. Rev. B* **5**, 4877 (1972).
- ²⁷V. Moruzzi, D. Teaney, and B. van der Hoeven Jr., *Solid State Communications* **6**, 461 (1968).
- ²⁸T. Kasuya and A. Yanase, *Rev. Mod. Phys.* **40**, 684 (1968).
- ²⁹M. Müller, R. Schreiber, and C. M. Schneider, *Magnetics, IEEE Transactions on* **47**, 1635 (2011).
- ³⁰M. Müller, R. Schreiber, and C. M. Schneider, *Journal of Applied Physics* **109**, 07C710 (2011).
- ³¹D. O'Mahony, C. Smith, C. Budtz-Jorgensen, M. Venkatesan, J. Lunney, J. McGilp, and J. Coey, *Thin Solid Films* **488**, 200 (2005).
- ³²M. P. Mulloy, W. J. Blau, and J. G. Lunney, *Journal of Applied Physics* **73**, 4104 (1993).
- ³³M. C. Franzblau, G. E. Everett, and A. W. Lawson, *Phys. Rev.* **164**, 716 (1967).
- ³⁴A. Tsukada, K. Luna, R. Hammond, M. Beasley, J. Zhao, and S. Risbud, *Applied Physics A* **104**, 311 (2011).
- ³⁵S. H. Risbud and Y.-H. Han, *Scripta Materialia* **69**, 105 (2013).
- ³⁶S. H. Risbud, J. R. Groza, and M. J. Kim, *Philosophical Magazine Part B* **69**, 525 (1994).
- ³⁷J. Zhao, T. Holland, C. Unuvar, and Z. A. Munir, *International Journal of Refractory Metals and Hard Materials* **27**, 130 (2009).
- ³⁸L. Van der Pauw, *Philips Tech. Rev.* **20**, 220 (1958).
- ³⁹G. J. Dolan and D. D. Osheroff, *Phys. Rev. Lett.* **43**, 721 (1979).
- ⁴⁰T. R. McGuire and M. W. Shafer, *Journal of Applied Physics* **35**, 984 (1964).
- ⁴¹R. Schiller and W. Nolting, *Solid State Communications* **110**, 121 (1999).
- ⁴²F. Huang, G. J. Mankey, M. T. Kief, and R. F. Willis, *Journal of Applied Physics* **73**, 6760 (1993).
- ⁴³F. Tsui, M. C. Smoak, T. K. Nath, and C. B. Eom, *Applied Physics Letters* **76**, 2421 (2000).
- ⁴⁴A. D. Fried, M. M. Fejer, and A. Kapitulnik, "A scanning, all-fiber sagnac interferometer for high resolution magneto-optic measurements at 820nm," To be published.
- ⁴⁵J. Xia, P. T. Beyersdorf, M. M. Fejer, and A. Kapitulnik, *Applied Physics Letters* **89**, 062508 (2006).
- ⁴⁶J. T. Cheung, D. B. Geohegan, and L.-C. Chen, *Pulsed Laser Deposition of Thin Films*, edited by D. B. Chrisey and G. K. Hubler (Wiley, 1994) Chap. 1, 5, 6.
- ⁴⁷H. Okamoto, "Eu-S Phase Diagram," in *Alloy phase diagrams center* (ASM International, 1990).
- ⁴⁸C. L. Yaws, *Yaws' Handbook of Properties of the Chemical Elements* (Knovel, 2011).
- ⁴⁹S. Metev and M. Sendova, "Thin-film compounds formation with pulsed laser-plasma fluxes," in *Third International Conference on Trends in Quantum Electronics* (European Physical Society, 1988) p. 260.
- ⁵⁰M. Galassi, J. Davies, J. Theiler, B. Gough, G. Jungman, P. Alken, M. Booth, and F. Rossi, *GNU Scientific Library: Reference Manual* (Network Theory Limited, 2009).
- ⁵¹T. Williams, C. Kelley, *et al.*, "gnuplot: An interactive plotting program," .